RAA 2014 Vol. **14** No. **7**, 855–863 doi: 10.1088/1674–4527/14/7/007
http://www.raa-journal.org *http://www.iop.org/journals/raa*

***R**esearch in*
***A**stronomy and*
***A**strophysics*

Numerical simulations of three-dimensional magnetic swirls in a solar flux-tube

Piotr Chmielewski[1], Krzysztof Murawski[1] and Alexandr A. Solov'ev[2]

[1] Group of Astrophysics, University of Maria Curie-Skłodowska, ul. Radziszewskiego 10, 20-031 Lublin, Poland; *p_chmielewski@yahoo.com*

[2] Pulkovo Astronomical Observatory, Pulkovskoe shosse 65/1, 196140, Saint Petersburg, Russian Federation

Received 2014 February 6; accepted 2014 May 7

Abstract We aim to numerically study evolution of Alfvén waves that accompany short-lasting swirl events in a solar magnetic flux-tube that can be a simple model of a magnetic pore or a sunspot. With the use of the FLASH code we numerically solve three-dimensional ideal magnetohydrodynamic equations to simulate twists which are implemented at the top of the photosphere in magnetic field lines of the flux-tube. Our numerical results exhibit swirl events and Alfvén waves with associated clockwise and counterclockwise rotation of magnetic lines, with the largest values of vorticity at the bottom of the chromosphere, and a certain amount of energy flux.

Key words: MHD — Sun: magnetic fields — Alfvén waves propagation

1 INTRODUCTION

Studies of vortex-like motions in the solar atmosphere are important since photospheric vortex motions are able to propagate upwards and influence the outer-atmospheric magnetic fields. With the advent of sophisticated detectors, small-scale spatial processes in the atmosphere of the Sun can be detected. Indeed, there are observed vortex-like motions of sunspots (Brown et al. 2003), eddies in photospheric granulation (Brandt et al. 1988) and whirlpool motions of magnetic bright points in the intergranular lanes (Bonet et al. 2008; Bonet et al. 2010). Recently, Wedemeyer-Böhm & Rouppe van der Voort (2009) discovered small, rotating swirls in the solar chromosphere. They interpreted their observations as plasma spiraling upwards in a funnel-like magnetic structure that can be an effect of wavefront propagation guided by magnetic field lines. Shelyag et al. (2011) investigated magnetic photospheric vortices and showed evidence of two different types of vortex motions in the solar photosphere: baroclinic motions of plasma in non-magnetic granules and vortices in strongly magnetized intergranular lanes, which can be responsible for excitation of different types of magnetohydrodynamic (MHD) wave modes. In their numerical model of the lower atmosphere with a three-dimensional (3D) open magnetic flux-tube model, Fedun et al. (2011) showed that high-frequency vortex motion in the photosphere, with a period of 30 s, is able to excite torsional Alfvén waves. The turbulent convection in subsurface layers results in magnetized vortex tubes, which produce small-scale eruptions (Kitiashvili et al. 2013). The pressure gradient and Lorentz forces inject subphotospheric plasma higher into the photosphere and upper layers of the solar atmosphere, contributing to solar plasma heating. Moreover, rotation of magnetic field lines is linked to coronal heating and solar flares (Parker 1988). Despite many observations and studies of swirls, their scenario still remains unexplored.

A goal of this paper is to contribute to the above mentioned studies by performing numerical simulations of the generation and evolution of magnetic swirls in the solar atmosphere. We use a model of a 3D gravitationally stratified magnetic flux-tube, which constitutes a simple model of a magnetic pore or a sunspot (Roberts & Webb 1978). A twist in magnetic lines implemented at the top of the photosphere excites swirls and Alfvén waves (Vasheghani Farahani et al. 2012).

This paper is organized as follows. A numerical model is presented in Section 2, and the corresponding numerical results are shown in Section 3. Our work is concluded by a summary of the numerical results in Section 4.

2 A NUMERICAL MODEL

Our model of a gravitationally-stratified solar atmosphere is described by the ideal, adiabatic, 3D MHD equations

$$\frac{\partial \varrho}{\partial t} + \nabla \cdot (\varrho \boldsymbol{V}) = 0\,, \tag{1}$$

$$\varrho \frac{\partial \boldsymbol{V}}{\partial t} + \varrho\,(\boldsymbol{V} \cdot \nabla)\,\boldsymbol{V} = -\nabla p + \frac{1}{\mu}(\nabla \times \boldsymbol{B}) \times \boldsymbol{B} + \varrho \boldsymbol{g}\,, \tag{2}$$

$$\frac{\partial p}{\partial t} + \nabla \cdot (p\boldsymbol{V}) = (1-\gamma) p \nabla \cdot \boldsymbol{V}\,, \qquad p = \frac{k_{\rm B}}{m} \varrho T\,, \tag{3}$$

$$\frac{\partial \boldsymbol{B}}{\partial t} = \nabla \times (\boldsymbol{V} \times \boldsymbol{B})\,, \qquad \nabla \cdot \boldsymbol{B} = 0\,. \tag{4}$$

Here ϱ is mass density, $\boldsymbol{V} = [V_x, V_y, V_z]$ the flow velocity, $\boldsymbol{B} = [B_x, B_y, B_z]$ the magnetic field, p is gas pressure, T temperature, $\gamma = 5/3$ the adiabatic index, $\boldsymbol{g} = (0, -g, 0)$ gravitational acceleration with $g = 274$ m s^{-2}, m is the mean particle mass that is specified by the mean molecular weight of 1.24, and $k_{\rm B}$ is Boltzmann's constant.

In Equations (1)–(4) we neglected non-ideal and non-adiabatic terms such as viscosity, magnetic diffusivity, thermal conduction, and plasma heating and cooling terms. The latter may play an important role in lower regions of the solar atmosphere and at the transition region. Dropped non-adiabatic effects of plasma heating and cooling are important in lower regions of the solar atmosphere. All neglected effects are not expected to qualitatively change the general behavior of waves, which are attenuated by non-ideal and non-adiabatic terms.

2.1 Equilibrium State

The solar atmosphere is assumed to be in static equilibrium ($\boldsymbol{V}_0 = \boldsymbol{0}$) with a Lorentz force balanced by the gravity force and the gas pressure gradient,

$$\frac{1}{\mu}(\nabla \times \boldsymbol{B}_0) \times \boldsymbol{B}_0 = \nabla p_0 - \varrho_0 \boldsymbol{g}\,. \tag{5}$$

Here $\boldsymbol{B}_0$, $\boldsymbol{V}_0$, ϱ_0 and p_0 denote equilibrium magnetic field, velocity, mass density and plasma pressure, respectively. We consider a 3D model of the Schlüter-Temesváry model (Low 1985) of a flux-tube. In this model $\boldsymbol{B}_0$ is defined by the magnetic flux function,

$$\boldsymbol{B}_0 = B_0 \exp(-u\phi) \left[\frac{\Lambda_0^2 z^2}{(a^2+r^2)^2}, \frac{\Lambda_0^2}{a^2+r^2} + B_{\rm ext}, -\frac{\Lambda_0^2 xz}{(a^2+r^2)^2} \right] , \tag{6}$$

where

$$\phi = \frac{r^2}{a^2+\bar{y}^2}, \quad r^2 = x^2 + z^2 , \tag{7}$$

$\bar{y} = y - 500$ km, $B_{\rm ext} \approx 11.4$ G is the external magnetic field and

$$\Lambda_0 = \frac{k_{\rm B} T_{\rm h}(y_{\rm r})}{mg} \tag{8}$$

is the pressure scale height evaluated at the reference level $y_{\rm r} = 10$ Mm in the solar corona. The symbol $T_{\rm h}(y)$ denotes a hydrostatic temperature for which we use the semi-empirical VAL-C model of plasma temperature (Vernazza et al. 1981). In this model the temperature reaches its minimum, $T_{\rm min} \sim 4300$ K, in the chromosphere at $y \sim 0.9$ Mm and it rapidly grows with height at the solar transition region, at $y \sim 2.7$ Mm, to $T \sim 1.5$ MK in the solar corona (not shown). The symbols a and u are free parameters, which we set as $a = 150$ km and $u \approx 0.43$, and hold them fixed. The reference magnetic field magnitude, B_0, is chosen in such a way that the magnetic field within the flux-tube, at $(x = 0, y = 0.5, z = 0)$ Mm, is about 10^3 G. This value corresponds to a moderately strongly magnetized flux-tube. Note that the magnetic field lines are predominantly vertical around the line $x = z = 0$ Mm, but further out they are bent in the form of the reversed bottle-shape profile (Fig. 1, left) and the magnitude of $\boldsymbol{B}_0$ decays with distance from this line.

Having specified the magnetic field, Equation (6), Low (1985) derived the equilibrium gas pressure, $p_0(y)$, and mass density, $\varrho_0(y)$, as

$$p_0(x,y,z) = p_{\rm h}(y) - p_0 \frac{\exp(-2u\phi)\Lambda_0^4}{2\beta(a^2+\bar{y}^2)^3} \left[2\left(\phi + 1 - \frac{1}{u}\right)(a^2+\bar{y}^2) + a^2\left(\frac{3}{u} - 2\phi\right)\right] , \tag{9}$$

$$\varrho_0(x,y,z) = \varrho_{\rm h}(y) - \varrho_0 \frac{\exp(-2u\phi)\Lambda_0^5}{2\beta(a^2+\bar{y}^2)^4} \left[8\left(\phi + 1 - \frac{1}{u}\right)\bar{y}(a^2+\bar{y}^2) + 6a^2\bar{y}\left(\frac{3}{u} - 2\phi\right)\right] , \tag{10}$$

where p_0 and ϱ_0 denote respectively the gas pressure and mass density at $y_{\rm r} = 10$ Mm, and β is the plasma beta, which is defined as the ratio of p_0 and the equilibrium magnetic pressure, $B_0^2/(2\mu)$. The plasma beta is evaluated at the point $(0, 10, 0)$ Mm, which is located within the solar corona. The subscript 'h' in Equations (9) and (10) corresponds to a hydrostatic gas pressure and the hydrostatic mass density, which are given by the following expressions:

$$p_{\rm h}(y) = p_0 \exp\left[-\int_{y_{\rm r}}^{y} \frac{dy'}{\Lambda(y')} \right] , \quad \varrho_{\rm h}(y) = \frac{p_{\rm h}(y)}{g\Lambda(y)} , \tag{11}$$

where

$$\Lambda(y) = \frac{k_{\rm B} T_{\rm h}(y)}{mg} \tag{12}$$

is the pressure scale height.

3 RESULTS OF NUMERICAL SIMULATIONS

We solve ideal, adiabatic MHD equations, specified by Equations (1)–(3) with the use of the FLASH code (Fryxell et al. 2000; Lee & Deane 2009; Lee 2013), which implements a second-order unsplit Godunov solver (e.g., Murawski & Tanaka 1997) with various slope limiters and Riemann solvers. We use the minmod slope limiter and approximate Harten-Lax-van Leer-Discontinuities (HLLD) Riemann solver (Lee 2013).

Our simulation box is set as $(-1.25, 1.25)\,\mathrm{Mm} \times (0.5, 15.5)\,\mathrm{Mm} \times (-1.25, 1.25)\,\mathrm{Mm}$. In all our studies we use a static but non-uniform grid with a minimum (maximum) level of refinement set to 3 (5), which results in the finest spatial resolution of $\Delta x = \Delta y = \Delta z = 19.5$ km. Each block in the numerical grid consists of $8 \times 8 \times 8$ identical numerical cells.

We impose boundary conditions by fixing all plasma quantities with respect to time at all boundaries to their equilibrium values. The only exception is the bottom boundary, where quantities at the boundary are excessively lagged due to implementing the azimuthal component of the magnetic field, B_θ, defined as

$$B_\theta(x, y, t) = \begin{cases} -b_\theta\, r\, \exp\left[-\frac{r^2+(y-y_0)^2}{w^2}\right]\left(\frac{t}{\tau}\right), & t \le \tau, \\ 1, & t > \tau, \end{cases} \tag{13}$$

where $b_\theta = 11.4$ G is the amplitude of the twist and $\tau = 200$ s is the duration of the growing time. The twist in the magnetic field is centered at the point $(0, 0.5, 0)$ Mm, which corresponds to the top of the photosphere. The growing time of the twist corresponds to a fast solar twist and aims to be the best representation of fast magnetic swirls observed in the solar atmosphere (Wedemeyer-Böhm & Rouppe van der Voort 2009; Kitiashvili et al. 2013). As a result of the twist (Eq. (13)), we observe upward propagation of torsional Alfvén waves, which are visible as twisted magnetic field lines (Fig. 1) and a circular plasma flow (Fig. 2). We observe rotational plasma motions generated at the top of the photosphere, at the level $y = 0.5$ Mm (Figs. 2 and 3). The upwardly propagating perturbation in plasma velocity grows slightly in amplitude with height. At $t = 200$ s $|V_z(x, y, z = 0)| \simeq 0.6$ km s^{-1}, while at $t = 400$ s $|V_z(x, y, z = 0)| \simeq 1.5$ km s^{-1}. The Alfvén waves leave the simulation domain, resulting in a slight rotation of plasma (Fig. 2, right).

Figure 3 illustrates the vorticity, $\Omega = V_\theta/r$, where V_θ is the angular velocity (Vasheghani Farahani et al. 2011). Note that Ω grows in altitude over time; at $t = 200$ s the signal in Ω reaches the altitude $y \approx 0.75$ Mm (left), while at $t = 500$ s it is already non-zero up to $y \approx 4$ Mm. Plasma rotation, which is associated with Alfvén waves, escalates and propagates upwardly along the magnetic field lines into the solar corona; at $t = 400$ s it reaches the transition region, undergoing a partial reflection from there (Fig. 2, left, and Fig. 3, middle). On the other hand, perturbations in the magnetic field, which are excited by the twist, evolve upwards up to the transition region where they are significantly reflected backwards down to lower atmospheric regions (Fig. 1, right). This reflection results from the significant gradient in mass density, which in turn causes a large variation in the Alfvén speed, in the transition region (not shown).

A bird's-eye view of magnetic lines, from the solar corona, at $y = 9$ Mm, down into the chromosphere and photosphere, is illustrated in Figure 4. We see rotation of the magnetic lines, which are associated with upwardly propagating Alfvén waves. At $t = 400$ s and $t = 440$ s, we observe Alfvén waves moving upwards and magnetic lines rotating clockwise. After the waves pass the altitude $y = 9$ Mm (Fig. 4, bottom-left), the magnetic lines start to rotate counterclockwise. This phenomenon was already described by a number of authors, e.g. by Nakariakov & Verwichte (2005), van Ballegooijen et al. (2011) and Hansen & Cally (2012).

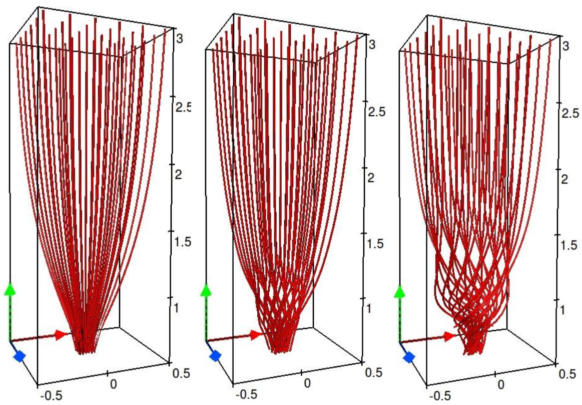

Fig. 1 Temporal snapshots of magnetic field lines at $t = 0$ s (*left*), $t = 300$ s (*middle*) and $t = 500$ s (*right*). Red, green and blue arrows correspond to the x-, y- and z-axes, respectively.

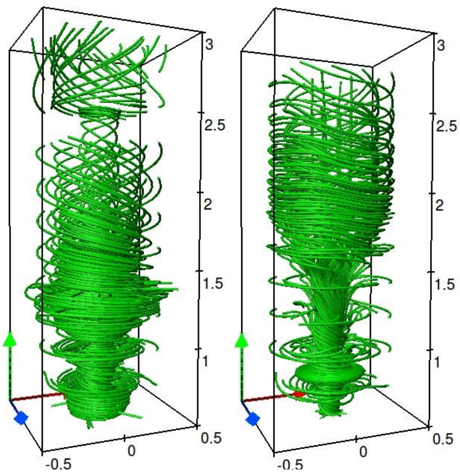

Fig. 2 Temporal snapshots of streamlines at $t = 400$ s (*left*) and $t = 900$ s (*right*). Red, green and blue arrows correspond to the x-, y- and z-axes, respectively.

We evaluate the energy flux using the following approximate relation, which is derived for linear Alfvén waves in a gravity-free medium (Vigeesh et al. 2012)

$$\boldsymbol{E}_{\mathrm{flux}} \approx \left[\varrho c_{\mathrm{A}} V_x^2, \varrho c_{\mathrm{s}} V_y^2, \varrho c_{\mathrm{A}} V_z^2\right], \tag{14}$$

where

$$c_{\mathrm{A}} = \frac{|\boldsymbol{B}|}{\sqrt{\mu\varrho}}, \qquad c_{\mathrm{s}} = \sqrt{\frac{\gamma p}{\varrho}}, \tag{15}$$

are Alfvén, sound and fast speeds, respectively. Figure 5 presents time-signatures of the energy flux. Panels (a), (b) and (c) contain the x-component (solid line), y-component (short-dashed line) and z-component (long-dashed line) of energy fluxes. Each panel corresponds to a different detection

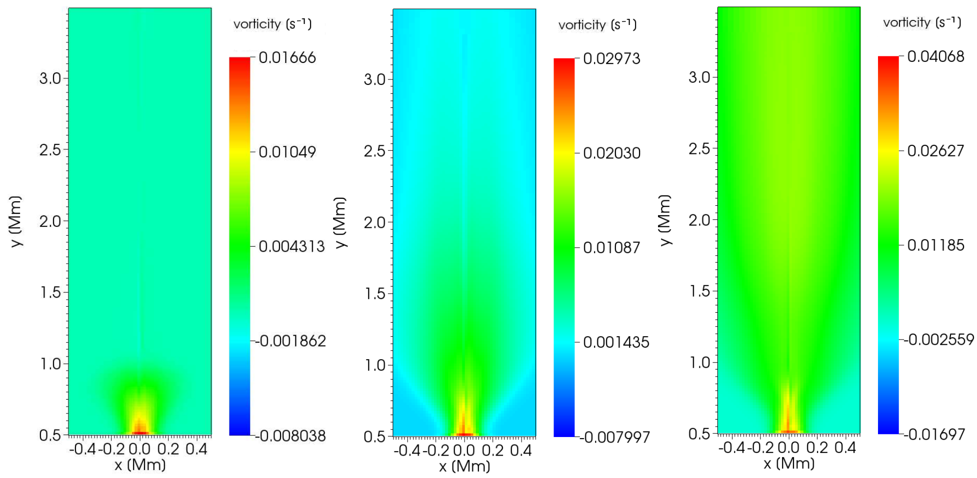

Fig. 3 Vorticity $\Omega = v_\phi / r$ profiles at $t = 200$ s (*left*), $t = 400$ s (*middle*) and $t = 500$ s (*right*), for $z = 0$ Mm.

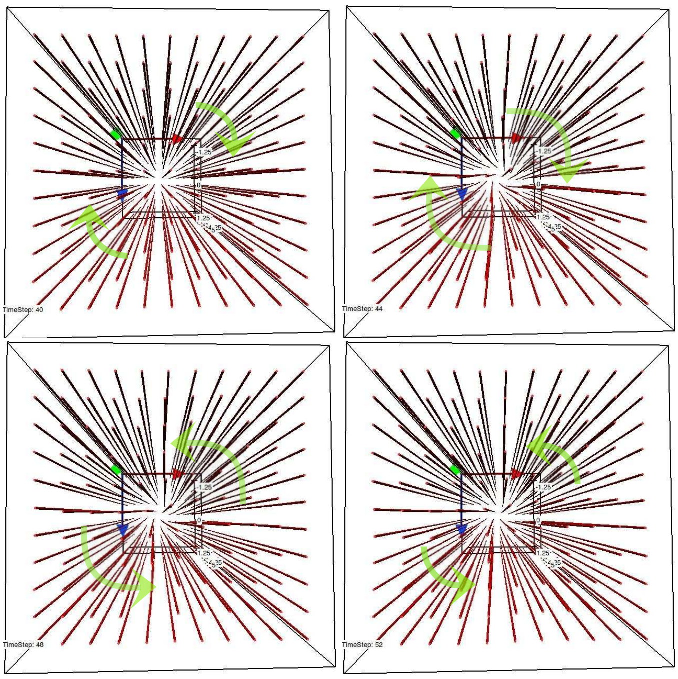

Fig. 4 Bird's-eye view (from the solar corona, at $y = 9$ Mm, down into the photosphere) of magnetic lines at $t = 400$ s, $t = 440$ s, $t = 480$ s and $t = 520$ s (from top-left to bottom-right). Red, green and blue thin arrows correspond to the x-, y- and z-axes, respectively. Thick green arrows show rotation of the magnetic field lines.

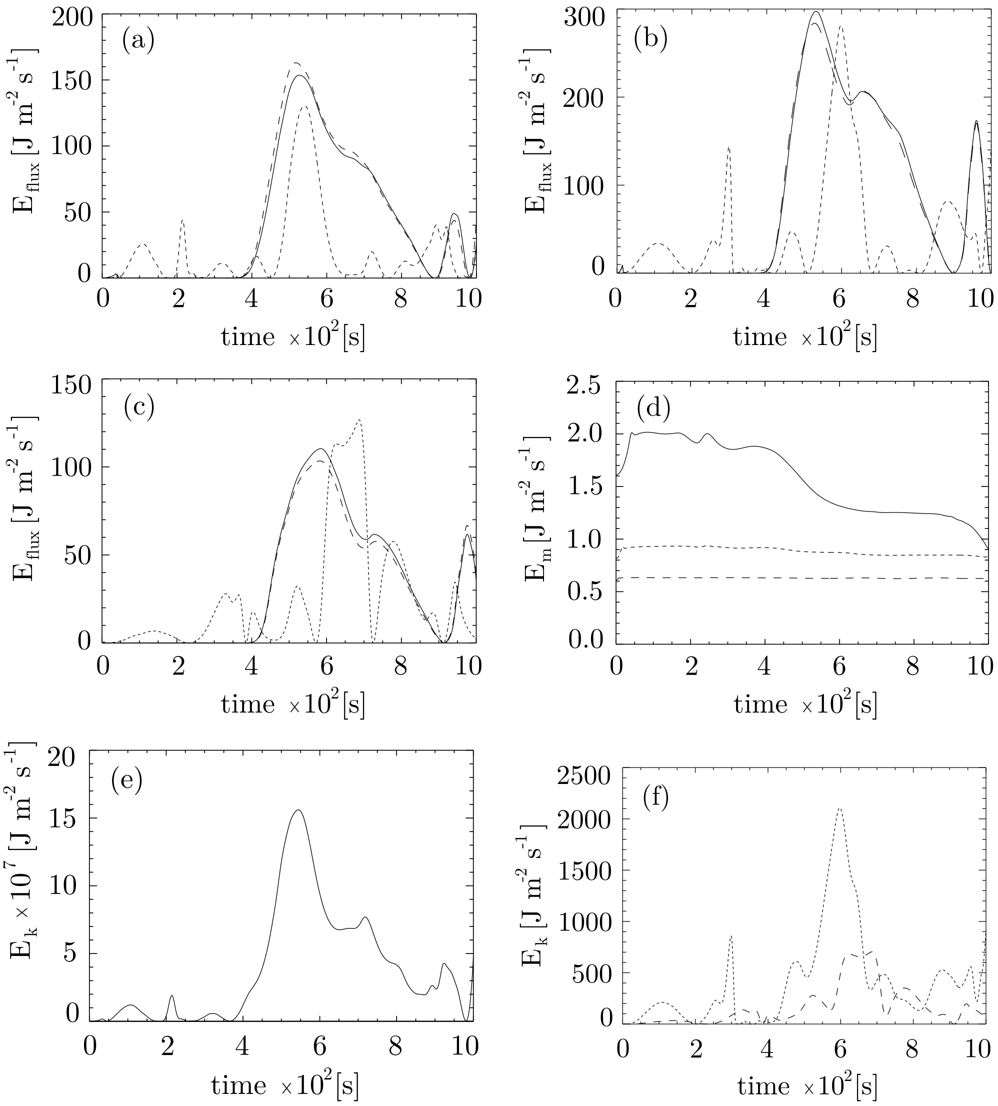

Fig. 5 Time-signatures of x- (*solid line*), y- (*short-dashed line*) and z-components (*long-dashed line*) of the energy flux collected at $y = 2$ Mm (a), $y = 3$ Mm (b) and $y = 4.5$ Mm (c), the magnetic energy (d) and kinetic energy (panels (e) and (f)) collected at fixed $x = z = 0.05$ Mm and at $y = 2$ Mm (*solid line*), $y = 3$ Mm (*short-dashed line*) and $y = 4.5$ Mm (*long-dashed line*).

point, which is located at $(x_0, y_0, z_0) = (0.05, 2, 0.05)$ Mm (a), $(x_0, y_0, z_0) = (0.05, 3, 0.05)$ Mm (b) and $(x_0, y_0, z_0) = (0.05, 4.5, 0.05)$ Mm (c).

In the upper chromosphere (a) x- and y-components of energy fluxes, F_x and F_z, vary in a similar way and reach a maximum value of about 160 J m^{-2} s^{-1} as the Alfvén waves pass the altitude $y = 2$ Mm (Fig. 5, panel a). Above the transition region, maximum values of x- and y-components of energy fluxes are about 300 J m^{-2} s^{-1} and 115 J m^{-2} s^{-1} for $y = 3$ Mm (Fig. 5, panel b) and $y = 4.5$ Mm (Fig. 5, panel c), respectively. Note that the energy flux of the order of a few hundred J m^{-2} s^{-1} is transferred through the transition region by the Alfvén waves, however it decreases with altitude.

On the other hand, when Alfvén waves are passing, the vertical component of the energy flux reaches its maximum of 130 J m^{-2} s^{-1} below the transition region (a), briefly varies above the transition region while increasing its value up to 280 J m^{-2} s^{-1} (b), and finally F_y reaches 130 J m^{-2} s^{-1} in the solar corona (c). The vertical component of the energy flux is able to heat a quiet corona, and it reaches $100 \sim 200$ J m^{-2} s^{-1} (Withbroe & Noyes 1977). The vertical flux results from the ponderomotive force exerted by the torsional Alfvén waves in the wave-guiding magnetic flux-tube (e.g., Vasheghani Farahani et al. 2011).

Panels (d)–(f) of Figure 5 show time-variation of the magnetic and kinetic energies collected at three different altitudes at $y = 2$ Mm (solid line), $y = 3$ Mm (short-dashed) and at $y = 4.5$ Mm (long-dashed line). We observe a decrease of the detected magnetic energy with height, which results from magnetic field lines that diverge and conservation of magnetic energy. Below the transition region (Fig. 5(e)), the kinetic energy attains a value of about 1.6×10^8 J m^{-3}, but above this region it does not exceed 2.2×10^3 J m^{-3} (Fig. 5(f)). Note that local changes in these energies are associated with temporal variation of plasma associated with passing Alfvén waves.

4 SUMMARY

In our 3D numerical model of a magnetically structured and gravitationally stratified solar atmosphere, we twist magnetic field lines at the top of the photosphere, exciting Alfvén waves, which propagate into the solar corona. The generated Alfvén waves are associated with vortex-like motions that are observed in the solar atmosphere (Brown et al. 2003; Bonet et al. 2008; Wedemeyer-Böhm et al. 2012). We describe the evolution of Alfvén waves in the flux-tube (Low 1985) and associated clockwise and counterclockwise rotation of magnetic field lines, as well as a significant amount of vorticity in the bottom layers of the chromosphere. While analyzing the flux-energy variation with height above and below the transition region, we found that Alfvén waves accompanying the twisted magnetic lines contribute to heating of the flux-tube.

Acknowledgements We express our thanks to the referee for his/her stimulating comments. This work was supported by the Marie Curie PIRSES-GA-295272-RADIOSUN project. The FLASH code was developed by the DOE-supported ASC Alliance Center for Astrophysical Thermonuclear Flashes at the University of Chicago.

References

Bonet, J. A., Márquez, I., Sánchez Almeida, J., Cabello, I., & Domingo, V. 2008, ApJ, 687, L131
Bonet, J. A., Márquez, I., Sánchez Almeida, J., et al. 2010, ApJ, 723, L139
Brandt, P. N., Scharmer, G. B., Ferguson, S., Shine, R. A., & Tarbell, T. D. 1988, Nature, 335, 238
Brown, D. S., Nightingale, R. W., Alexander, D., et al. 2003, Sol. Phys., 216, 79
Fedun, V., Shelyag, S., Verth, G., Mathioudakis, M., & Erdélyi, R. 2011, Annales Geophysicae, 29, 1029
Fryxell, B., Olson, K., Ricker, P., et al. 2000, ApJS, 131, 273
Hansen, S. C., & Cally, P. S. 2012, ApJ, 751, 31
Kitiashvili, I. N., Kosovichev, A. G., Lele, S. K., Mansour, N. N., & Wray, A. A. 2013, ApJ, 770, 37
Lee, D. 2013, Journal of Computational Physics, 243, 269
Lee, D., & Deane, A. E. 2009, Journal of Computational Physics, 228, 952
Low, B. C. 1985, ApJ, 293, 31
Murawski, K., & Tanaka, T. 1997, Ap&SS, 254, 187
Nakariakov, V. M., & Verwichte, E. 2005, Living Reviews in Solar Physics, 2, 3

Parker, E. N. 1988, ApJ, 330, 474
Roberts, B., & Webb, A. R. 1978, Sol. Phys., 56, 5
Shelyag, S., Fedun, V., Keenan, F. P., Erdélyi, R., & Mathioudakis, M. 2011, Annales Geophysicae, 29, 883
van Ballegooijen, A. A., Asgari-Targhi, M., Cranme, S. R., & DeLuca, E. E. 2011, ApJ, 736, 3
Vasheghani Farahani, S., Nakariakov, V. M., van Doorsselaere, T., & Verwichte, E. 2011, A&A, 526, A80
Vasheghani Farahani, S., Nakariakov, V. M., Verwichte, E., & Van Doorsselaere, T. 2012, A&A, 544, A127
Vernazza, J. E., Avrett, E. H., & Loeser, R. 1981, ApJS, 45, 635
Vigeesh, G., Fedun, V., Hasan, S. S., & Erdélyi, R. 2012, ApJ, 755, 18
Wedemeyer-Böhm, S., & Rouppe van der Voort, L. 2009, A&A, 507, L9
Wedemeyer-Böhm, S., Scullion, E., Steiner, O., et al. 2012, Nature, 486, 505
Withbroe, G. L., & Noyes, R. W. 1977, ARA&A, 15, 363